Volume 3 | Number 17 | 7 May 2015 | Pages 4207–4586

Journal of Materials Chemistry C

Materials for optical, magnetic and electronic devices

www.rsc.org/MaterialsC

ISSN 2050-7526

ROYAL SOCIETY OF CHEMISTRY

COMMUNICATION

Zhengqi Liu, Guiqiang Liu *et al.*

Enhancing refractive index sensing capability with hybrid plasmonic–photonic absorbers

Journal of
Materials Chemistry C

COMMUNICATION

Cite this: J. Mater. Chem. C, 2015, 3, 4222

Received 21st December 2014,
Accepted 5th March 2015

DOI: 10.1039/c4tc02928c

www.rsc.org/MaterialsC

Enhancing refractive index sensing capability with hybrid plasmonic–photonic absorbers

Zhengqi Liu,* Meidong Yu, Shan Huang, Xiaoshan Liu, Yan Wang, Mulin Liu, Pingping Pan and Guiqiang Liu*

We experimentally report an enhanced refractive index sensor with a maximum figure of merit (FOM*) value of about 1337 based on a hybrid plasmonic–photonic absorber *via* utilizing a substantial absorption contrast between a perfect absorber (~99% at normal incidence) and a non-perfect absorber when there are changes in their surroundings.

Surface plasmon resonance (SPR) originates from the coherent electron oscillation of metallic structures. The interaction of light with SPRs can be controlled to yield surprising optical properties, and this has been a well-established and a highly sensitive technique for label-free real-time sensing,[1–6] having wide applications in refractive index (RI) detection and[7–10] environment-related concerns such as the detection of flammable gases[11–13] and chemical reactions.[14–16] In all the areas mentioned above, the simultaneous detection of small quantities with a high spectral intensity contrast is desirable. Furthermore, a sensing platform with a simple structure is also important for real applications. Therefore, all sensors have to be evaluated first with respect to their sensitivity on marginal changes in their surroundings. Localized surface plasmon resonances (LSPRs) in plasmonic nanostructures have the potential to provide these properties.[17–22] The resonant electric field surrounding the nanostructure can associate the spectral wavelength of the resonances to the RI of their surroundings. Based on the precise functionalization of the structural geometries, spatially selective plasmon sensing can be obtained.[23,24] In particular, structures with small gaps not only provide a great enhancement in sensitivity but also are most efficient in optical and electrical trapping[25,26] and sensing detection.[24,27] Because of the demand of high accuracy for fabricating such nanometer separated structures, scanning beam techniques, including electron beam lithography[28] and focused ion beam lithography,[29] are the main fabrication methods. However, for a cheaper translation into practical devices, the high requirements of these fabrication techniques inevitably limit their further applications. Moreover, the fabrication of other plasmonic structures with high sensitivity and high spectral intensity contrast, which explores the relationship between the sensing properties and structures and makes use of them, is still in progress.

Recently, extensive investigations have been conducted to develop nanoplasmonic sensors based on the extraordinary optical transmission (EOT) through periodic nanoaperture arrays in metallic films[30–34] or metallic film coated colloidal crystals (M-CCs).[35–38] M-CCs have novel fabrication features due to the simple colloidal self-assembly method[39–41] and the standard metal film deposition technique, which have been proposed to be utilized as alternative platforms for the plasmon sensing scheme. For instance, an impressive plasmon sensing based on large-area M-CCs was achieved in the visible spectrum.[42] In addition, because a colloidal crystal (CC) assisted approach has a patterning capability to produce surface-confined arrays of plasmonic films with a tunable structural size at a low cost using simple methods, this plasmon sensing scheme can be easily adjusted to different frequencies.[38,43] Nevertheless, the figure of merit (FOM*) for the relative spectral intensity changes was always small due to the intrinsic broadband resonant spectrum,[38,43] which directly counteracts the high spectral shifts and leads to a low spectral intensity contrast. Therefore, it has been an open question for an appropriate way for improving the FOM* of these CC-assisted plasmonic sensors.

In this letter, we theoretically propose and experimentally demonstrate the feasibility of a significantly improved plasmon sensing platform by utilizing a substantial absorption contrast between a perfect absorber (~99% at normal incidence) and a non-perfect absorber when there are changes in the refractive index. Besides the relatively high spectral wavelength shift sensitivity, an excellent spectral intensity contrast with a maximal FOM* of up to 1337 was obtained in the near-infrared region.

Fig. 1 illustrates a schematic of the hybrid plasmonic–photonic absorber consisting of three functional layers including a

Laboratory of Nanomaterials and Sensors, College of Physics and Communication Electronics, Key Laboratory of Optoelectronic and Telecommunication of Jiangxi Province, Jiangxi Normal University, Nanchang 330022, China.
E-mail: zliu@jxnu.edu.cn, liugq@jxnu.edu.cn; Fax: +86 0791 88120370;
Tel: +86 0791 88120370

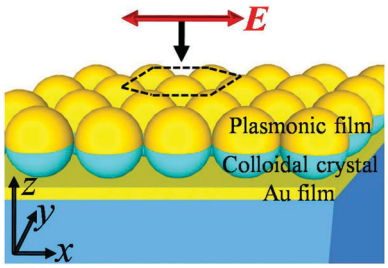

Fig. 1 Schematic of the hybrid plasmonic–photonic absorber.

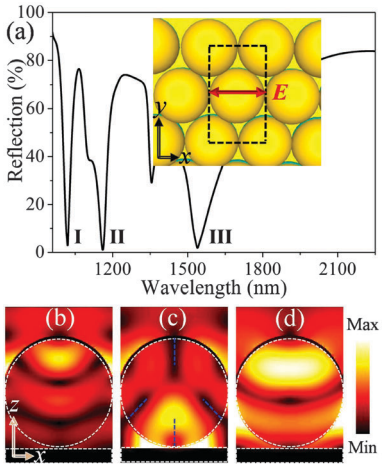

Fig. 2 (a) Calculated reflection of the structure under a normal illumination. The inset diagram shows the calculation unit cell (dashed rectangle) for the periodic crystal structure. (b)–(d) Normalized electric field intensity distributions for the resonances at 1020 nm (I), 1162 nm (II), and 1538 nm (III), respectively.

conventional M-CC with a 30 nm gold plasmonic film coated on the top of a two dimensional CC and a 100 nm-thick gold film substrate. The dashed hexagon (Fig. 1) indicates the hexagonal-close-packed crystal structure. Herein, the CC consists of 1080 nm polystyrene (PS) spheres. For the M-CC, EOT phenomenon can be obtained at certain wavelength ranges due to a coupling between the excited plasmon resonances of the plasmonic film and the photonic guided modes including the cavity resonance of the CC.[38] The introduction of an opaque Au film can not only cancel the light transmission but also introduce SPRs due to the grating scattering of the CC.[44–46] Three-dimensional numerical simulations were conducted using a finite-difference time-domain method.[47] The calculation domain in the *xoy* plane constitutes one complete and four quarter metallic shells and PS spheres. Periodic boundary conditions were applied to the four sides of the calculation domain to mimic the periodicity of the whole structure. Perfect matching layers were used in the direction of *z*-axis to completely absorb the scattering field. The lattice period of the M-CC was equal to the diameter of the original PS microsphere, *i.e.*, $P = 1080$ nm. The refractive index of the PS was taken as 1.59, and the permittivity of gold was described by a Drude model, $\varepsilon_{gold} = 1 - \omega_p^2/[\omega(\omega + i\omega_c)]$, with a plasma frequency $\omega_p = 2\pi \times 2.175 \times 10^{15}$ s^{-1} and collision frequency $\omega_c = 2\pi \times 6.5 \times 10^{12}$ s^{-1}.[48] Considering the grain boundary effect, surface scattering, and inhomogeneous broadening in the thin film, the damping constant used in the calculations was about three times as large as that in bulk gold.[49]

Fig. 2 presents the calculated reflection spectrum and the corresponding normalized electric field intensity distributions of the main absorption resonances. Four sharp anti-reflection bands were observed, as shown in Fig. 2(a). For the formation of these reflection dips, the contributions from the top corrugated metallic film, the middle CC and the bottom Au film should be considered. For instance, the photonic guided modes can be excited based on the monolayer CC under illumination, which can couple with the incident electromagnetic fields and produce a slight anti-reflection spectrum.[38] Sharp reflection dips can be obtained due to the excitation of the SPRs and guided modes for the opaque Au film coated with a monolayer CC.[45] For the corrugated plasmonic film, the excitation of the localized plasmon resonances, including the dipolar and multi-polar plasmon resonances, provides a broadband optical coupling with the incident light.[35–38,50] Because the hybrid plasmonic–photonic absorber consists of the abovementioned three parts, the plasmonic resonances supported by the metallic films, the optical modes supported by the CC and their hybridizations should be considered for the absorption mechanism. For the resonance at 1020 nm (I), the electric field was mainly confined to the area that was close to the corrugated metallic film and the CC (Fig. 2(b)), which indicates that the excitation of the dipolar plasmon resonance and the guided mode were the main contribution to the absorption. At 1162 nm (II), a strong electric field was observed in the gap areas between the CC and the Au film, which confirms the excitation of the SPR.[45] In addition, an obvious electric field intensity was also observed in the areas close to the top corrugated metallic film and the spheres, where four obvious field nodes could be clearly seen in the sphere indicated by the dashed line (Fig. 2(c)). Such a field pattern suggests the excitation of the quadrupolar plasmons.[38] Therefore, the excitation of the SPR and the quadrupolar plasmons of the corrugated metallic film were the main contributions to the absorption band. At 1538 nm (III), an obvious optical field was concentrated by the spheres (Fig. 2(d)), which confirms the excitation of the guided mode of the CC.[45] The field pattern indicates that the absorption at this wavelength was the main result of the optically guided coupling and trapping.

Experimental fabrication for this hybrid plasmonic–photonic absorber includes three procedures. First, a 100 nm-thick Au film was deposited onto a clean silica glass. Then, a hexagonal-close-packed CC was self-assembled on the Au coated glass, which had been functionalized with hydrophilic molecules. Finally, a 30 nm-thick Au film was deposited on this CC *via* a sputtering method. As shown in Fig. 3(a), a uniform colorimetric response on a large-area sample was achieved based on these well-developed and standard techniques, which indicates the feasibility of fabrication with low-cost and high-reproducibility for this type of absorber.[36–39] Cross-view scanning electron microscopy (SEM) image is presented in Fig. 3(b), which shows that the M-CC was uniformly packed on the flat Au film. The top-view SEM of the sample is shown in Fig. 3(c), which shows that a highly ordered

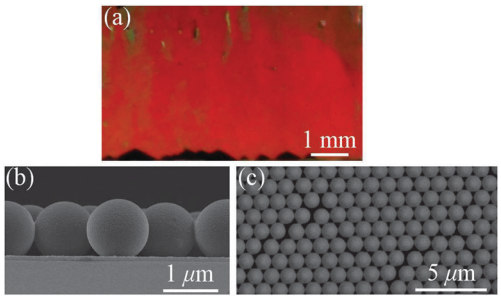

Fig. 3 (a) Optical image of the fabricated hybrid plasmonic–photonic absorber. Cross-view (b) and top-view (c) SEM images of the structure.

CC was generally achieved, though there were some disorders or mismatching parts that were randomly located in the sample.

A reflectance (R) spectrum was obtained by dividing the reflection intensity of our sample by that of a gold-coated mirror. Incident light with an 8-mm diameter spot was used as the illumination source. Fig. 4(a) shows the measured reflection spectrum of the sample under an almost normal illumination ($\sim 7^\circ$ of the incident angle). Ultra-low reflection values of 0.06% (1097 nm, λ_1), 0.77% (1234 nm, λ_2), and 0.96% (1596 nm, λ_3) were achieved. Because the light transmission (T) was completely inhibited by the opaque Au film, the absorbance (A) can be defined as $A = 1 - R$ ($T = 0$). Therefore, a near-unity multispectral absorption ($A > 99\%$) was realized in this hybrid plasmonic–photonic structure. Thus, an entire high-absorption spectrum with absorptivity above 99% was achieved for this multi-band absorber. In comparison with the multiple sharp anti-reflection bands in the calculated model, the observed broadened and high-absorption spectrum in the experiment could be the main result of the inevitably existing disorder and the multi-domain of the crystal structure during the fabrication process. In fact, the partial disorder not only leads to a strongly broadened bandwidth of the resonant spectrum but also provides other appropriate channels for the coupling of light due to the wide size dispersion of the unit cells because of the randomly packed spheres with a series of geometry parameters.[51,52]

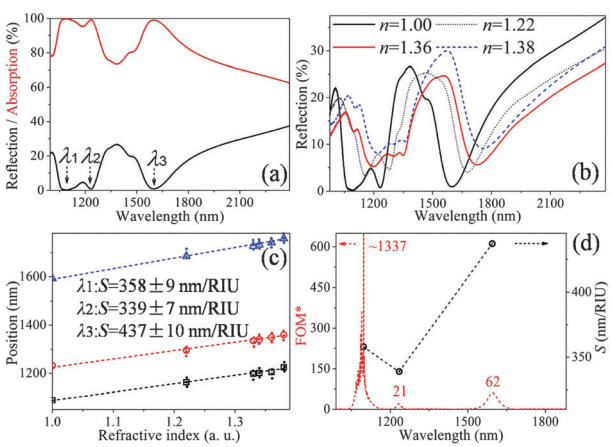

Fig. 4 (a) Experimental reflection and absorption spectra of the hybrid plasmonic–photonic absorber. (b) Reflection spectra for the sample under different surrounding media. (c) Resonance wavelengths as a function of the RI of the surrounding medium. (d) FOM* and S as a function of wavelength.

Fig. 4(b) presents the measured spectra of the sample that is surrounded with different RI environments. It was observed that the spectral curves of the sample under different surroundings not only show obvious wavelength shifts but also produce a strong spectral intensity modulation. For instance, when n was 1.36, the reflection dip (λ_3) moved to 1728 nm and the reflectance increased to 5.6%. Thus, besides the conventional wavelength shift detection for the plasmon sensing, the strong spectral intensity changes, which are caused by the different surroundings, would provide great contributions towards a high-quality sensing because the real detection was mostly based on the display of intensity caused by the photoelectric conversion during the spectral measurement.

The repeated spectral measurement of the reflection dips were plotted as a function of the RI of the surrounding medium. As shown in Fig. 4(c), the sensitivity (S) values of λ_1–λ_3 were as high as 358 ± 9 nm/RIU, 339 ± 7 nm/RIU, and 457 ± 10 nm/RIU, respectively. These results are remarkable when compared with most of the plasmonic nanostructure-based sensors and planar metamaterial LSPR sensors.[11] In addition, in comparison with a sensitivity of less than 200 nm/RIU for the conventional M-CCs,[38] sensitivities larger by two-fold were achieved for this plasmon sensing scheme.

The sensing capability of the hybrid plasmonic–photonic absorber can be examined by evaluating the figure of merit, which is typically defined as FOM = S/FWHM, where S represents the bulk wavelength sensitivity (denoted as $\Delta\lambda$/RIU) and FWHM represents the spectral full-width at half maximum. This definition allows the plasmonic nanostructures to be judged against one another because sensing platforms are independent of their shape and size.[53] Alternatively, a relative intensity change, dI/I, of the resonance spectrum at a fixed wavelength, λ_0, because of a small index change dn can also be detected, especially in the situation in which the plasmonic resonance does not follow a simple Lorentzian peak. Furthermore, the relative spectral intensity change can produce a more meaningful information when a real optoelectronic measurement is carried out using the transformation from the photonics to the electrics under a certain spectral intensity difference.[11] Therefore, an alternative figure of merit (FOM*), which was introduced by J. Becker *et al.*,[54] was defined as FOM* = d$I(\lambda)$/d$n(\lambda)$/$I(\lambda)$, where $I(\lambda)$ is the intensity in air and d$I(\lambda)$ is the intensity change induced by a change in the refractive index dn. According to this definition, a sharp reflectance dip with a narrow line width is as crucial as a small reflection intensity, and the maximum value of FOM* can be obtained around the perfect absorption frequency.[11] Fig. 4(d) presents the experimental FOM* for ethanol (with a dn of 0.36) as a function of wavelength. The maximal value of FOM* for the absorption peak (λ_1) was around 1337. Compared to the experimental FOM* of plasmonic gold nanorods,[55] which is around 24, FOM* by this technique was considerably higher. Moreover, in comparison with the FOM* with a value of 87 for a well-designed infrared plasmonic perfect absorber,[11] the enhancement factor for this hybrid plasmonic–photonic absorber was up to 15. The fundamental advantage of our absorber sensor lies in the fact that it allows the detection of photons that are reflected by the

non-perfect absorber upon a change in RI *versus* a nearly dark reference measurement, where only a few photons are reflected from the perfect absorber. For an optimum operation, specific care is usually given to reduce the background intensity due to scattering as well as due to detector noise. Herein, the excellent contrast signal ratio for the spectral intensity difference before and after the situation with RI medium automatically insures a high-quality detection. For the three resonances (namely, λ_1–λ_3), the experimentally determined S in terms of wavelength shift per refractive index unit (RIU) was above 300 nm/RIU, which is compatible with excellent current LSPR sensor data. It is also noteworthy that our sensor design is highly scalable and can be tuned to the visible or gigahertz frequency regions by appropriately tuning the sizes of the sphere.

In conclusion, we have experimentally demonstrated a hybrid plasmonic–photonic absorber in the near-infrared region. Compared with the common EOT phenomenon supported by the conventional M-CC, a multi-band near-unity light absorption was achieved for this structure. In particular, this absorber can work as an RI sensor with a high FOM*. The combination of the basic sensing principles and particular physical phenomena can open up a new pathway for plasmonic sensing and will facilitate a new class of microscopic sensors. Importantly, the presented sensing strategy has general applicability for a large variety of nanofabrication technologies. It has profound significance for developing cheap and easily available sensing equipment in which only common self-assembled and deposition techniques for structural fabrication together with the simple measurement technologies for detection are needed. Therefore, the sensing platform demonstrated in this study provides potential applications in improving the performance of plasmonic refractive index sensors and developing a future surface enhanced multi-spectral infrared absorption.

Acknowledgements

This work was supported by the National Natural Science Foundation of China (Grant 11464019 and 11264017), Natural Science Foundation of Jiangxi Province (Grants 20142BAB212001), Young Scientist development program of Jiangxi Province (Grant 20142BCB23008), Project of Jiangxi Provincial Education Department (Grant GJJ14253) and Projects of Jiangxi Normal University (Grants 5460 and 6047).

Notes and references

1 J. N. Anker, W. P. Hall, O. Lyandres, N. C. Shah, J. Zhao and R. P. Van Duyne, *Nat. Mater.*, 2008, **7**, 442.
2 S. Zeng, D. Baillargeat, H.-P. Ho and K.-T. Yong, *Chem. Soc. Rev.*, 2014, **43**, 3426.
3 Y. Gao, Z. Xin, B. Zeng, Q. Gan, X. Cheng and F. J. Bartoli, *Lab Chip*, 2013, **13**, 4755.
4 J. Homola, S. S. Yee and G. Gauglitz, *Sens. Actuators, B*, 1999, **54**, 3; H.-J. Qiu, X. Li, H.-T. Xu, H.-J. Zhang and Y. Wang, *J. Mater. Chem. C*, 2014, **2**, 9788.
5 S. Yang, D. Slotcavage, J. D. Mai, F. Guo, S. Li, Y. Zhao, Y. Lei, C. E. Cameronc and T. J. Huang, *J. Mater. Chem. C*, 2014, **2**, 8350.
6 Y. Gao, Q. Gan, Z. Xin, X. Cheng and F. J. Bartoli, *ACS Nano*, 2011, **5**, 9836.
7 S. Seo, M. R. Gartia and G. L. Liu, *Nanoscale*, 2014, **6**, 11795.
8 B. Zeng, Y. Gao and F. J. Bartoli, *Nanoscale*, 2015, **7**, 166.
9 X. Wu, J. Zhang, J. Chen, C. Zhao and Q. Gong, *Opt. Lett.*, 2009, **34**, 392.
10 N. Liu, M. Mesch, T. Weiss, M. Hentschel and H. Giessen, *Nano Lett.*, 2010, **10**, 2342.
11 M. G. Manera, G. Montagna, E. Ferreiro-Vila, L. González-García, J. R. Sánchez-Valencia, A. R. González-Elipe, A. Cebollada, J. M. Garcia-Martin, A. Garcia-Martin, G. Armelles and R. Rella, *J. Mater. Chem.*, 2011, **21**, 16049.
12 B. Liedberg, C. Nylander and I. Lunström, *Sens. Actuators*, 1983, **4**, 299.
13 L. Polavarapu, J. Pérez-Juste, Q.-H. Xu and L. M. Liz-Marzán, *J. Mater. Chem. C*, 2014, **2**, 7460.
14 H. Jans and Q. Huo, *Chem. Soc. Rev.*, 2012, **41**, 2849.
15 J. Homola, *Chem. Rev.*, 2008, **108**, 462.
16 K. A. Willets and R. P. Van Duyne, *Annu. Rev. Phys. Chem.*, 2007, **58**, 267.
17 E. Kazuma and T. Tatsuma, *Nanoscale*, 2014, **6**, 2397.
18 Y. Zhan, D. Y. Lei, X. Li and S. A. Maier, *Nanoscale*, 2014, **6**, 4705.
19 B. Ai, L. Wang, H. Möhwald, Y. Yu and G. Zhang, *Nanoscale*, 2015, **7**, 2317.
20 S. Szunerits and R. Boukherroub, *Chem. Commun.*, 2012, **48**, 8999.
21 C. Wang, Q. Zhang, Y. Song and S. Y. Chou, *ACS Nano*, 2014, **8**, 2618.
22 Y. Gao, Q. Gan and F. J. Bartoli, *IEEE J. Sel. Top. Quantum Electron.*, 2014, **20**, 6900306.
23 Z. Liu, H. Shao, G. Liu, X. Liu, H. Zhou, Y. Hu, X. Zhang, Z. Cai and G. Gu, *Appl. Phys. Lett.*, 2014, **104**, 081116.
24 I. Ament, J. Prasad, A. Henkel, S. Schmachtel and C. Sonnichsen, *Nano Lett.*, 2012, **12**, 1092.
25 A. Kotnala and R. Gordon, *Nano Lett.*, 2014, **14**, 853.
26 D. Punj, M. Mivelle, S. B. Moparthi, T. S. van Zanten, H. Rigneault, N. F. van Hulst, M. F. García-Parajó and J. A. Wenger, *Nat. Nanotechnol.*, 2013, **8**, 512.
27 E. Altewischer, C. Genet, M. P. van Exter, J. P. Woerdman, P. F. A. Alkemade, A. van Zuuk and E. W. J. M. van der Drift, *Opt. Lett.*, 2005, **30**, 90.
28 B. Brian, B. Sepulveda, Y. Alaverdyan, L. M. Lechuga and M. Kaell, *Opt. Express*, 2009, **17**, 2015.
29 T. W. Ebbesen, H. J. Lezec, H. F. Ghaemi, T. Thio and P. A. Wolff, *Nature*, 1998, **391**, 667.
30 W. Yue, Z. Wang, Y. Yang, J. Li, Y. Wu, L. Chen, B. Ooi, X. Wang and X. Zhang, *Nanoscale*, 2014, **6**, 7917.
31 X. Zhang, Z. Li, S. Ye, S. Wu, J. Zhang, L. Cui, A. Li, T. Wang, S. Li and B. Yang, *J. Mater. Chem.*, 2012, **22**, 8903.
32 V. Canpean and S. Astilean, *Lab Chip*, 2009, **9**, 3574.
33 C. Heo, H. C. Jeon, S. Y. Lee, S. G. Jang, S. Cho, Y. Choi and S. Yang, *J. Mater. Chem.*, 2012, **22**, 13903.

34 Y. Shen, X. Chen, Z. Dou, N. P. Johnson, Z.-K. Zhou, X. Wang and C. Jin, *Nanoscale*, 2012, **4**, 5576.

35 L. Landström, D. Brodoceanu, D. Bäuerle, F. J. García-Vidal, S. G. Rodrigo and L. Martín-Moreno, *Opt. Express*, 2009, **17**, 761.

36 S. G. Romanov, A. V. Korovin, A. Regensburger and U. Peschel, *Adv. Mater.*, 2011, **23**, 2515.

37 P. Zhan, Z. L. Wang, H. Dong, J. Sun, H. T. Wang, S. N. Zhu, N. B. Ming and J. Zi, *Adv. Mater.*, 2006, **18**, 1612.

38 Z. Liu, J. Hang, J. Chen, Z. Yan, C. Tang, Z. Chen and P. Zhan, *Opt. Express*, 2012, **20**, 9215.

39 J. Xiao, L. Yang, Y. Luo, D. Li and Q. Meng, *J. Mater. Chem. C*, 2013, **1**, 5450.

40 H. Xu, P. Wu, C. Zhu, A. Elbaza and Z. Z. Gu, *J. Mater. Chem. C*, 2013, **1**, 6087.

41 I. B. Burgess, M. Lončarb and J. Aizenberg, *J. Mater. Chem. C*, 2013, **1**, 6075.

42 Y. Y. Li, J. Sun, L. Wang, P. Zhan, Z. S. Cao and Z. L. Wang, *Appl. Phys. A: Mater. Sci. Process.*, 2008, **92**, 291.

43 Y. Y. Li, J. Pan, P. Zhan, S. N. Zhu, N. B. Ming, Z. L. Wang, W. D. Han, X. Y. Jiang and J. Zi, *Opt. Express*, 2010, **18**, 3546.

44 J. Grandidier, D. M. Callahan, J. N. Munday and H. A. Atwater, *Adv. Mater.*, 2011, **23**, 1272.

45 X. D. Yu, L. Shi, D. Z. Han, J. Zi and P. V. Braun, *Adv. Funct. Mater.*, 2010, **20**, 1910.

46 Z. Liu, P. Zhan, J. Chen, C. Tang, Z. Yan, Z. Chen and Z. L. Wang, *Opt. Express*, 2013, **21**, 3021.

47 A. Taflove and S. C. Hagness, *Computational Electrodynamics: the Finite-Difference Time-Domain Method*, Artech House, 2000.

48 M. A. Ordal, L. L. Long, R. J. Bell, S. E. Bell, R. R. Bell, R. W. Alexander Jr and C. A. Ward, *Appl. Opt.*, 1983, **22**, 1099.

49 N. Liu, L. Langguth, T. Weiss, J. Kästel, M. Fleischhauer, T. Pfau and H. Giessen, *Nat. Mater.*, 2009, **8**, 758.

50 Z. Liu, H. Shao, X. Liu, J. Chen, M. Liu, G. Fu, H. Xu and G. Liu, *Mater. Lett.*, 2014, **134**, 165.

51 Y. Yao, J. Yao, V. K. Narasimhan, Z. C. Ruan, C. Xie, S. H. Fan and Y. Cui, *Nat. Commun.*, 2012, **3**, 664.

52 K. Vynck, M. Burresi, F. Riboli and D. S. Wiersma, *Nat. Mater.*, 2012, **11**, 1017.

53 L. J. Sherry, S.-H. Chang, G. C. Schatz, R. P. Van Duyne, B. J. Wiley and Y. Xia, *Nano Lett.*, 2005, **5**, 2034.

54 J. Becker, A. Truegler, A. Jakab, U. Hohenester and C. Soennichsen, *Plasmonics*, 2010, **5**, 161.

55 N. Liu, T. Weiss, M. Mesch, L. Langguth, U. Eigenthaler, M. Hirschner, C. Sŏnnichsen and H. Giessen, *Nano Lett.*, 2009, **10**, 1103.

